Pflugers Arch - Eur J Physiol (2014) 466:1831–1844
DOI 10.1007/s00424-013-1414-x

MOLECULAR AND CELLULAR MECHANISMS OF DISEASE

Modeling of Friedreich ataxia-related iron overloading cardiomyopathy using patient-specific-induced pluripotent stem cells

Yee-Ki Lee · Philip Wing-Lok Ho · Revital Schick · Yee-Man Lau · Wing-Hon Lai · Ting Zhou · Yanhua Li · Kwong-Man Ng · Shu-Leung HO · Miguel Angel Esteban · Ofer Binah · Hung-Fat Tse · Chung-Wah Siu

Received: 18 July 2013 / Revised: 7 November 2013 / Accepted: 28 November 2013 / Published online: 11 December 2013

Abstract Friedreich ataxia (FRDA), a recessive neurodegenerative disorder commonly associated with hypertrophic cardiomyopathy, is due to GAA repeat expansions within the first intron of the frataxin (*FXN*) gene encoding the mitochondrial protein involved in iron–sulfur cluster biosynthesis. The triplet codon repeats lead to heterochromatin-mediated gene silencing and loss of frataxin. Nevertheless, inadequacy of existing FRDA-cardiac cellular models limited cardiomyopathy studies. We tested the hypothesis that iron homeostasis deregulation accelerates reduction in energy synthesis dynamics which contributes to impaired cardiac calcium homeostasis and contractile force. Silencing of *FXN* expressions occurred both in somatic FRDA-skin fibroblasts and two of the induced pluripotent stem cells (iPSC) clones; a sign of stress condition was shown in FRDA-iPSC cardiomyocytes with disorganized mitochondrial network and mitochondrial DNA (mtDNA) depletion; hypertrophic cardiac stress responses were observed by an increase in α-actinin-positive cell sizes revealed by FACS analysis as well as elevation in brain natriuretic peptide (BNP) gene expression; the intracellular iron accumulated in FRDA cardiomyocytes might be due to attenuated negative feedback response of transferring receptor (TSFR) expression and positive feedback response of ferritin (FTH1); energy synthesis dynamics, in terms of ATP production rate, was impaired in FRDA-iPSC cardiomyocytes, which were prone to iron overload condition. Energetic insufficiency determined slower Ca^{2+} transients by retarding calcium reuptake to sarcoplasmic reticulum (SR) and impaired the positive inotropic and chronotropic responses to adrenergic stimulation. Our data showed for the first time that FRDA-iPSCs cardiac derivatives represent promising models to study cardiac stress response due to impaired iron homeostasis

Yee-Ki Lee and Philip Wing-Lok Ho contributed equally to this work.

Electronic supplementary material The online version of this article (doi:10.1007/s00424-013-1414-x) contains supplementary material, which is available to authorized users.

Y.-K. Lee · Y.-M. Lau · W.-H. Lai · K.-M. Ng · H.-F. Tse · C.-W. Siu
Cardiology Division, Department of Medicine, Li Ka Shing Faculty of Medicine, the University of Hong Kong, Hong Kong, China

P. W.-L. Ho · S.-L. HO
Neurology Division, Department of Medicine, Li Ka Shing Faculty of Medicine, the University of Hong Kong, Hong Kong, China

R. Schick · O. Binah
Department of Physiology, The Sohnis Family Stem Cells Center, Technion - Israel Institute of Technology, Haifa, Israel

R. Schick · O. Binah
Department of Physiology, The Rappaport Family Institute for Research in the Medical Sciences, Technion - Israel Institute of Technology, Haifa, Israel

R. Schick · O. Binah
Department of Physiology, Ruth & Bruce Rappaport Faculty of Medicine, Technion - Israel Institute of Technology, Haifa, Israel

T. Zhou · Y. Li · M. A. Esteban
Stem Cell and Cancer Biology Group, Key Laboratory of Regenerative Biology, South China Institute for Stem Cell Biology and Regenerative Medicine, Guangzhou Institutes of Biomedicine and Health, Chinese Academy of Sciences, Guangzhou, China

C.-W. Siu (✉)
Department of Medicine, Queen Mary Hospital, The University of Hong Kong, Rm 1929A, Block K, Hong Kong, China
e-mail: cwdsiu@hku.hk

condition and mitochondrial damages. The cardiomyopathy phenotype was accelerated in an iron-overloaded condition early in calcium homeostasis aspect.

Keywords Friedreich ataxia · Induced pluripotent stem cells · Cardiomyopathy

Introduction

Friedreich ataxia (FRDA) is the most common hereditary ataxia. While the hallmark of the disease is progressive gait and limb ataxia [8, 28], most FRDA patients eventually develop cardiomyopathy that often leads to heart failure and premature cardiac death [22]. Genetically, FRDA is caused by GAA triplet repeat expansions within the first intron of the frataxin (*FXN*) gene encoding the mitochondrial protein frataxin, resulting in heterochromatin-mediated silencing of *FXN* in affected individuals [5, 9]. Although such genetic mutations are carried by as many as 96 % of FRDA patients [36], the pathogenic mechanisms linking the genetic defects to the development of cardiomyopathy and clinical heart failure remain largely inferential. It is now commonly accepted that frataxin plays an important role in mitochondrial iron metabolism particularly in the biosynthesis of iron–sulfur cluster, which is an essential component of many cellular enzymes and proteins [20, 24, 27]. In this regard, it has also been consistently demonstrated in endomyocardial biopsies obtained from FRDA patients the deficiency in mitochondrial iron–sulfur-dependent respiratory chain enzymes (mitochondrial electron transport complexes I, II, and III) and aconitase [2, 27]. Nonetheless, while conceptually plausible, direct experimental evidence to support the notion that deficiency of these enzymes and possibly the associated disruption of energy production contribute to the mechanical dysfunction of the myocardium and the development of clinical cardiomyopathy remain limited. On the other hand, frataxin deficiency increases cellular iron uptake via upregulation of transferrin receptor 1 (TfR1) resulting in excessive iron accumulation [12, 33]. In fact, iron overload has been documented in the hearts of FRDA patients [16, 21] as well as in mouse models of FRDA [6]. However, whether myocardial iron overload has a causal role in the disease pathogenesis remains to be determined [25]. Direct functional characterization of human cardiac tissues from FRDA patients can provide much needed insights to the pathogenesis, and such studies are limited by obvious ethical and technical reasons. Hence, the lack of appropriate-yet-reliable cellular disease model has hampered a systemic analysis of the pathogenesis and/or functional validation of candidate drugs.

The ability to generate disease-specific-induced pluripotent stem cells (iPSC) by reprogramming terminally differentiated human skin fibroblasts with four pivotal genes Oct3/4, Sox2, Klf4, and c-Myc [31, 34] can provide opportunities to recapitulate cardiac disease process in human tissue in vitro, as well as to develop a new therapeutic strategy [18, 30, 35]. Recently, FRDA-iPSC have been successfully generated and provided a cellular model system for mechanistic studies of repeat instability in FRDA [19]. Here we report the use of cardiomyocytes derived from FRDA-iPSC to elucidate the pathogenic role of iron overload in FRDA-related cardiac dysfunction.

Methods

Generation of human-induced pluripotent stem cells and their cardiac derivatives

For the generation of iPSC, we recruited a female FRDA patient with documented GAA triplet repeat expansions within the first intron of the frataxin (*FXN*) gene and one healthy age- and sex-matched control subject. The study protocol of procurement of human tissue for the generation of iPSCs was approved by the local Institutional Review Board and was registered at the Clinical Trial Center, the University of Hong Kong (HKCTR-725, http://www.hkclinicaltrials.com). Detailed methods on human iPSC generation and characterization and in vitro cardiac differentiation have been previously reported and are provided in the Supplementary Appendix.

Iron loading assay

To study the effects of iron loading, iPSC-derived cardiomyocytes were cultured for 48 h in a medium supplemented with 100 μM iron (II) sulfate from a stock solution at a concentration of 100 mM prepared by dissolving iron (II) sulfate in 0.1 % bovine serum albumin (BSA) in Dulbecco's phosphate buffered saline (DPBS) at pH 5.5. The iron content of cardiomyocytes was assayed with fluorescence quenching of calcein by iron. The dissociated cardiomyocytes from iPSCs were plated onto a 96-well white plate. Calcein-AM (Life Technologies, MD, USA) was dissolved in DMSO with a stock concentration of 10 mM. The dissociated cardiomyocytes were incubated in 10 μM calcein-AM in 5 % FBS cardiomyocyte maintenance medium for 15 min and washed twice with fresh medium before recording by M200 plate reader (Tecan, Männedorf, Switzerland) for every 5 s. The intracellular iron (II) ion levels were expressed as reciprocal of the initial rate of fluorescence intensity rise.

Reactive oxygen species (ROS) assay

Two million of WT- and FRDA-hiPSC cardiomyocytes were seeded into a 96-well black plate the day before the experiment. The cells were treated with iron (II) sulfate as previously described for 48 h. On day of the experiment, assay was performed using DCFDA Cellular ROA Detection Assay Kit (Abcam, Cambridge, UK) according to the manufacturer's instruction. In brief, the buffer solution, supplemented buffer, and HCFDA mix were freshly prepared. The cells were firstly washed by DPBS once and incubated with DCFDA mix for 45 min at 37 °C in the dark. A column of nonstained cells was reserved as blank control. Before measurement, the plate was washed once with buffer solution. The signal was then detected by M200 plate reader (Tecan, Männedorf, Switzerland) with excitation wavelength at 485 nm and emission at 535 nm.

Measurement of mitochondrial ATP synthesis activity by luciferin/luciferase bioassay

To meaure mitochondrial ATP production, cardiomyocytes seeded on a 96-well white plastic culture plate were permeabilized using streptolysin O (SLO) (Abcam, Cambridge, UK) to eliminate cytosolic content [7]. The cells were recovered and washed twice with DPBS. A permeabilization buffer (pH 7.3, calibrated by KOH, 25 mM HEPES–KOH, 125 mM potassium acetate, 2.5 mM magnesium acetate, and 1 mM DTT) containing activated SLO (1:100) was added and shaken on ice for 10 min. The cells were further washed twice by transportation buffer (pH 7.4, calibrated by KOH with 25 mM HEPES–KOH, 115 mM potassium acetate, 2.5 mM $MgCl_2$, 1 mM DTT, 2 mM EGTA, and protease inhibitor cocktail (Roche)) and incubated at 37 °C for 45 min. To start the ATP synthesis reaction, the cells preincubated with 5 mM succinate were treated with 100 μl phosphate buffer (25 mM Tris–HCl pH 7.4–7.5, 159 mM KCl, 2 mM EDTA, 0.1 % BSA, $MgCl_2$, and 10 mM KH_2PO_4) with a mixture of a substrate containing 1 mM ADP, 5 mM $MgCl_2$, 5 mM succinate, and 1× luciferin/luciferase mixture provided in ATP Bioluminescence Assay Kit CLSII (Roche Applied Science, Indianapolis, USA). The luminescence was measured every 5 s by M200 plate reader (Tecan, Männedorf, Switzerland). The kinetics of ATP synthesis was calculated as the initial upstroke rate of luminescence signal normalized with the protein amount in each well.

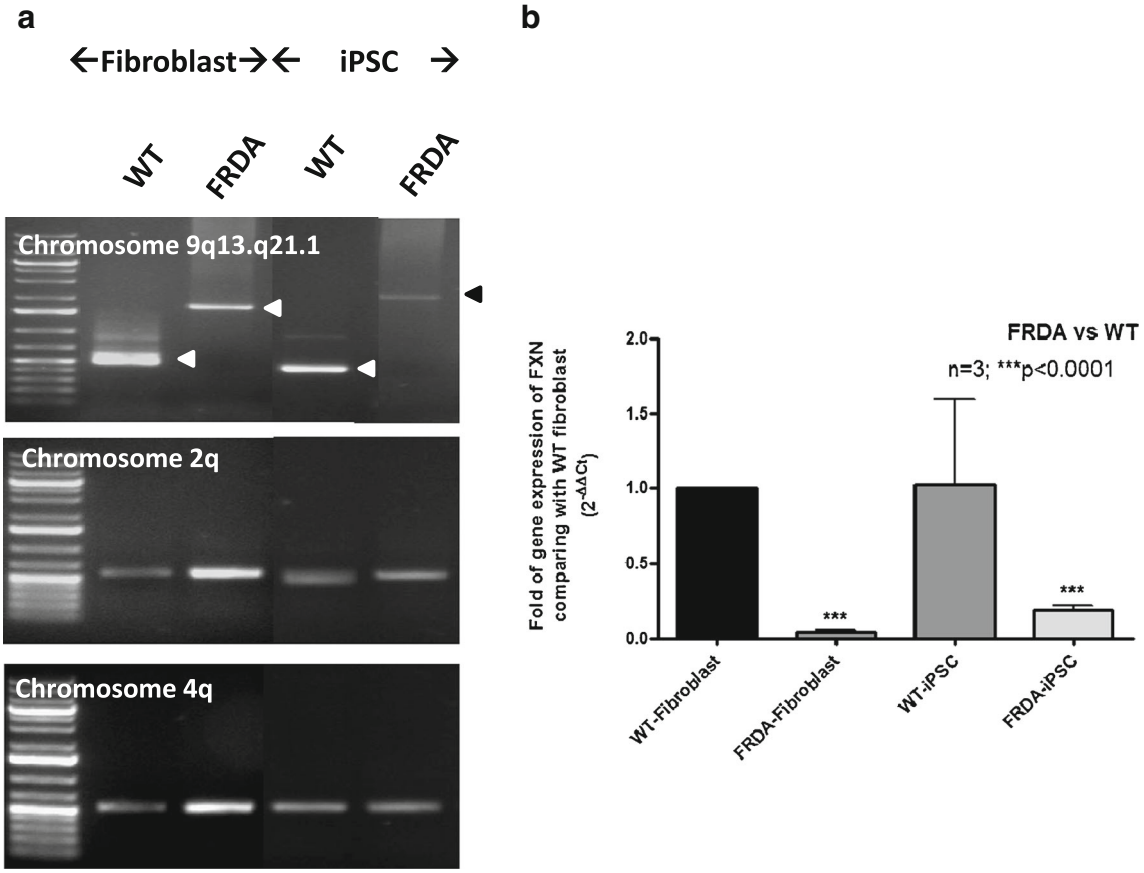

Fig. 1 **a** Analysis of the FXN intronic GAA triplet repeats to examine repeat length instability. Apparent expansions of FXN alleles (triplet repeat length more than 600, i.e., ~1.8 kb in intron 1) occurred in FRDA-fibroblast as well as iPSC. In contrast, the wild-type *FXN* allele of fibroblast and iPSC does not show any alternation is the size of GAA repeats (~600 bp). **b** Corresponding FXN gene silencing in FRDA-fibroblast and iPSC (WT vs. FRDA; $n=3$, $^{***}p<0.0001$)

Measurement of intracellular calcium homeostasis

Calcium handling kinetics was measured using our previously established protocol [17] (details are shown in Supplemental methods). Beta-adrenergic responses of the calcium transients were measured by the addition of isoprenaline (10 μM). In order to minimize contamination of the measurements by time-dependent changes in calcium handling properties in culture, all confocal calcium imaging experiments were performed within 48 h after cardiomyocyte dissociation.

Statistical analysis

Results were expressed as mean±SEM. Means of two populations were compared using Student's *t* test for paired observations. Two-way analysis of variance (ANOVA) was performed followed by Holm–Sidak test for all pairwise multiple comparison procedures, using SPSS (version 14.0). A value of $p < 0.05$ was considered significantly different.

Results

Generation of FRDA-iPSC

The first step was to establish primary cultures of dermal fibroblasts from a 35-year-old female FRDA patient with typical neurological features as well as clinical heart failure and from a control individual. Next, the fibroblasts were reprogrammed into human iPSCs using our previously published protocol [15]. Altogether two clones of iPSCs were generated from the FRDA-fibroblasts. The authenticity of these human iPSC lines was confirmed with contemporary standards (Supplementary data). As we did not detect any significant clone-to-clone variations in subsequent experiments, for description purposes, the data presented was the average of the two FRDA-iPSC clones. Analysis of *FXN* GAA triplet repeats by PCR revealed an expansion of FRDA alleles (triplet repeat length more than 600, i.e., ~1.8 kb) in FRDA-dermal fibroblasts but not in wild-type (WT) fibroblasts (Fig. 1a). In addition, apparent expansion of *FXN* GAA triplet was noted in FRDA-iPSCs after successful reprogramming, which was in contrast to WT-iPSC, whose numbers of *FXN* GAA triplet repeats remained the same as in their parent fibroblasts (Fig. 1a). However, no significant difference of *FXN* gene expression level was detected between with FA–fibroblast and iPSC (Fig. 1b). To verify that the observed GAA triplet repeat expansion in FRDA-fibroblasts and FRDA-iPSCs occurred specifically in the intronic region of *FXN*, PCR of the GAA repeats at two other unrelated loci (2q36, 16 repeats and 4q31.1, 30 repeats [26]) were tested and were found not to differ from WT cells (Fig. 1a). Further, the expression of *FXN* in FRDA-iPSCs was reduced by 80 % compared to WT-iPSC lines (Fig. 1b).

Cardiomyocytes derived from FRDA-iPSC

Following cardiac differentiation, spontaneously beating outgrowths were typically observed ~4 to 21 days in embryoid bodies from both FRDA- and WT-iPSC. Immunofluorescence analysis revealed typical patterns of a panel of cardiac-specific proteins: α-actinin, tropomyosin, and troponin-T in beating cells derived from both FRDA- and WT-iPSC at day 28, confirming their cardiac identity (Fig. 2a). To study mitochondrial network, cardiomyocytes derived from FRDA- and WT-iPSC were loaded with MitoROS staining. In WT-iPSC-CM, mitochondria were regularly spaced and located in positions interacting with the cytoskeleton actinin myofilaments

Fig. 2 **a** Generation of FRDA-iPSC-derived cardiomyocytes. The cardiac identities of the cardiac cells differentiated were defined by staining of cytoskeletal alpha-actinin, tropomysin, and troponin-T (cTnT); **b** disorganized network of mitochondrial distribution in FRDA-iPSC cardiomyocytes. The mitochondria mostly did not co-localize in sarcomere network as revealed by co-staining of alpha-actinin and mitoROS. Energy supply for cardiomyocyte contraction may be retarded; **c** Representative electron microscopy of WT- and FRDA-iPSC cardiomyocytes. Typical features of cardiac cells were shown with junctions at intercalated disc connecting adjacent cells and bundles of myofilaments assembled by Z banding. Highly organized myofilaments which form myofibrils were observed in WT-iPSC cardiomyocytes or myofibrils lacking alignment were shown in FRDA-iPSC cardiomyocytes. *Line graphs* reveal qualitative analysis of sarcomere organization which was appreciated as pixel intensity along a longitudinal axis line of cells. The control CMCs display regular oscillations between high and low intensities, representing well-organized sarcomeres. Mitochondria are highly abundance in FRDA-cardiac cells as observed in high-power field of cardiac cell under electron microscopy (*mt* mitochondria, *Z* Z bands of sarcomere, *J* junction, *tt* t-tubules); **d** significantly declined copy number of mitochondrial (mtDNA) in FRDA-iPSC cardiomyocytes as revealed by quantitative real-time PCR ($n=3$, $^{***}p<0.0001$). The mtDNA copy number is normalized to beta-globin gene expressed in the DNA samples extracted from beating embryoid bodies derived from WT- and FRDA-iPSCs. **E** Hypertrophic phenotypes of FRDA-iPSC cardiomyocytes under iron overload condition. The cardiomyocytes in the differentiated population were indicated by alpha-actinin-positive staining (PE) (gate on region F). The PE-positive cells (gate on region G) were further subjected to side scatter (SS) vs. forward scatter (FS) analysis. **f** The sizes of cardiomyocyte cell were expressed as the mean FS of the cell population shown in region G. Significant difference was tested by unpaired *t* test ($n=4$). **g** Gene expression of cardiac hypertrophic markers, BNP expression. **h** Iron overload in FRDA-iPSC cardiomyocytes. The level of intracellular iron (II) ion content is inversely proportional to the signal fluorescence dye, calcein-AM, since a high amount of divalent iron ions will quench the fluorescence signal. The rate of intracellular iron accumulation is calculated by 1/fluorescence signal of calcein (FLU)/protein amount of cell lysate (μg)/time (min). Iron loading in FRDA-iPSC-CMC is significantly higher when it is treated with an extreme amount of Fe^{2+} (100 μM) ($^{**}p<0.005$; $n=5$). **i** Synthesis of reactive oxygen species (ROS) in FRDA-iPSC cardiomyocytes. Iron loading (100 μM) in FRDA-iPSC-CMC caused a significant production in ROS indicating elevated oxidative stress ($^{**}p<0.0001$; $n=6$)

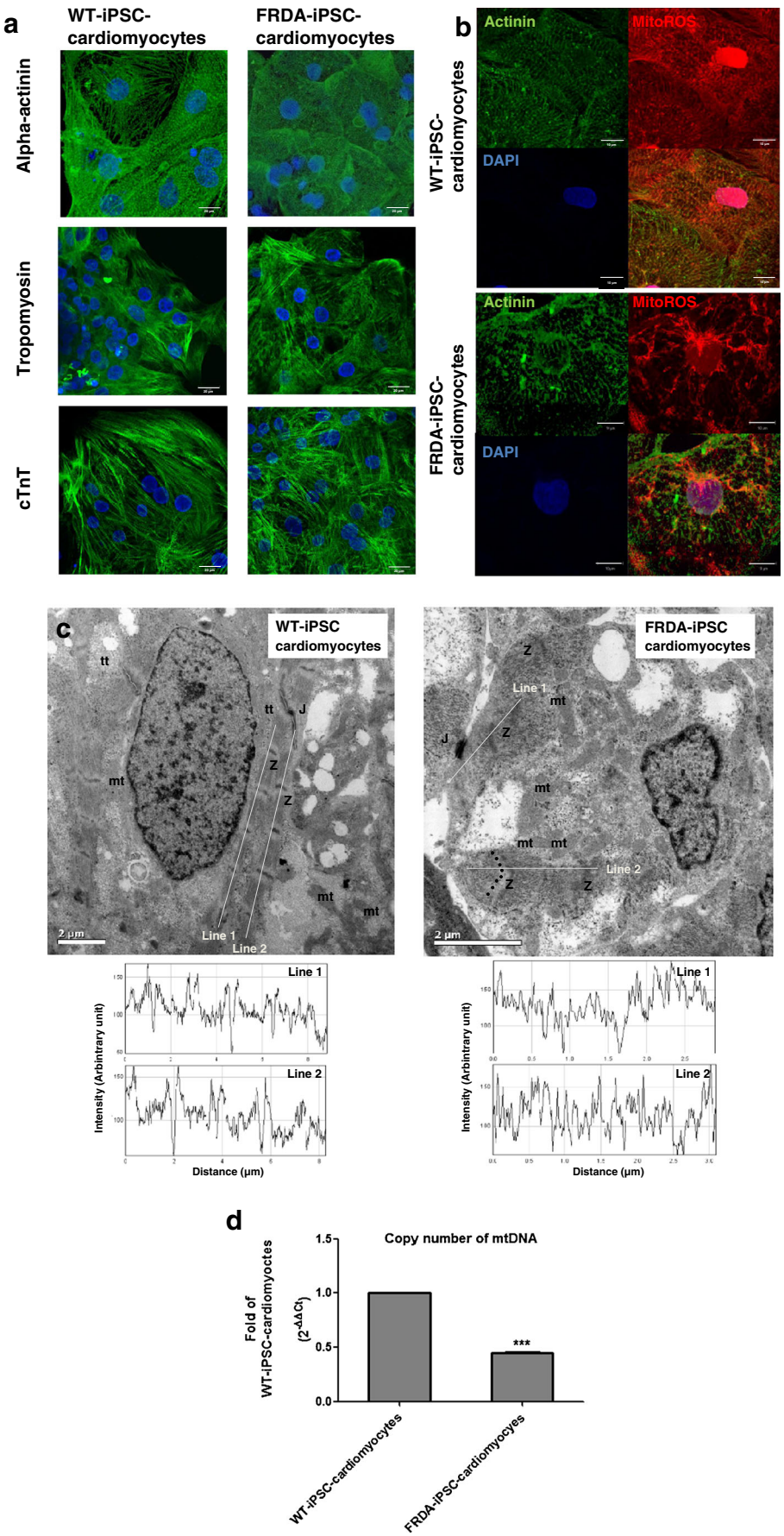
a
WT-iPSC-cardiomyocytes
FRDA-iPSC-cardiomyocytes
Alpha-actinin
Tropomyosin
cTnT
b
Actinin
MitoROS
DAPI
WT-iPSC-cardiomyocytes
FRDA-iPSC-cardiomyocytes
c
WT-iPSC cardiomyocytes
FRDA-iPSC cardiomyocytes
tt
J
Z
mt
Line 1
Line 2
2 µm
Intensity (Arbitrary unit)
Distance (µm)
d
Copy number of mtDNA
Fold of WT-iPSC-cardiomyocytes ($2^{-\Delta\Delta Ct}$)
1.5
1.0
0.5
0.0
***
WT-iPSC-cardiomyocytes
FRDA-iPSC-cardiomyocytes

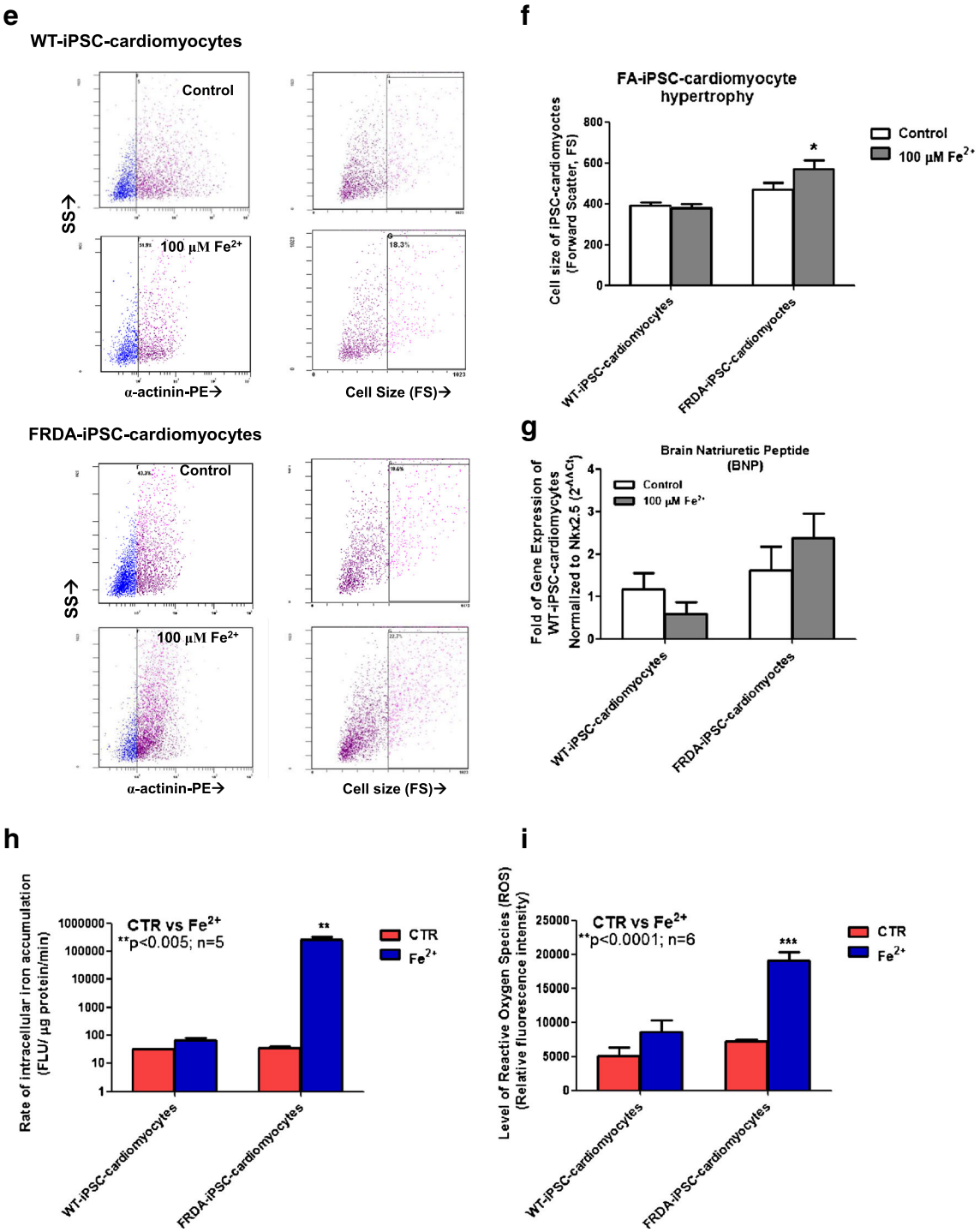

Fig. 2 (continued)

(Fig. 2b). In contrast, mitochondria in FRDA-iPSC-cardiomyocytes formed a disorganized, filamentous mitochondrial network without clear co-localization with actinin myofilaments. Interestingly, the copy number of mitochondrial DNA in FRDA-iPSC-derived cardiomyocytes was only 56 % of WT-iPSC-derived cardiomyocytes (Fig. 2d). Furthermore, ultrastructural alterations were also observed in FRDA-iPSC cardiomyocytes using electronic microscopy (Fig. 2c). Specifically, while sarcromere structure with highly organized myofilaments aligned with little shift between adjacent myofilament motifs and prominent Z banding was observed in WT-iPSC-derived cardiomyocytes, marked disarray of myofilaments was observed in FRDA-iPSC cardiomyocytes as highlighted by the black dots (Fig. 2c). The quantitative

transverse line analysis reveals regular oscillations between high- and low-contrast intensities observed in controls cardiac sarcomere, while FRDA-cardiac sarcomere displayed Z band misalignments, irregularities, and breakdowns.

Hypertrophic changes and altered iron homeostasis mechanism in FRDA-iPSC-derived cardiomyocytes

Because hypertrophic cardiomyopathy affects nearly all FRDA patients, we sought to determine whether the size of cardiomyocytes derived from FRDA-iPSC was larger than that of the WT counterparts; to our surprise, the size of cardiomyocytes from both groups was similar (Fig. 2e, f). Since it was suggested that iron loading plays an important pathogenic role in the development of hypertrophic cardiomyopathy in FRDA [3, 16, 27], we supplemented the cardiomyocyte culture medium with 100 μM iron (II) sulfate for 48 h. The cellular iron content in these cardiomyocytes was measured using a microplate assay based on the fluorescence quenching of calcein by iron (Fig. 2h). At baseline, iron content was similar in FRDA-iPSC and WT-iPSC cardiomyocytes (32.25±1.14 vs. 35.24±6.83 fluorescence light unit (FLU)/μg protein/min, $n=6$, respectively). However, iron loading for 48 h which increased cellular iron content in FRDA-iPSC-CM by ~7,500-folds was observed, while iron content remained unchanged in WT-iPSC-derived cardiomyocytes. Iron overloading in FRDA-hiPSC cardiomyocytes was accompanied with significantly elevated reaction oxygen species (ROS) production (Fig. 2h) (control vs. Fe^{2+}, 7,188±308 vs. 19,047±1,249 fluorescence intensity; $n=6$, ***$p<0.0001$). Intriguingly, while in FRDA-iPSC-CM, iron loading increased cell size by 16.6 % ($n=3$; *$p<0.05$), no change was observed in WT cells (Fig. 2e, f). Furthermore, the expression of brain natriuretic peptide (a cardiac stress marker) was upregulated by iron loading in FRDA-iPSC-derived cardiomyocytes, but not in WT cells (Fig. 2g). To further decipher the molecular basis of enhanced iron uptake, gene expression of the key proteins for iron transportation, transferin receptor (TSFR), iron-responsive element binding protein (IRP)-1 and IRP-2, ferroportin (FPN), and divalent metal transporter (DMT) was quantified and compared between FRDA-iPSC-CM and WT-iPSC-derived cardiomyocytes. At basal culture condition, the expression of TSFR, a transferrin-bound iron uptake protein, was similar in both groups (Fig. 3a). While iron loading suppressed the expression of TSFR in both FRDA (relative expression from 0.87±0.08 to 0.38±0.05, $p<0.001$) and WT-iPSC cardiomyocytes (0.97±0.02 to 0.21±0.03, $p<0.001$), FRDA-iPSC-derived cardiomyocytes are significantly to be less sensitive than WT cells to iron loading to TSFR suppression (WT iron-treated vs. FRDA iron-treated group, $n=4$; *$p<0.05$) (Fig. 3a). However, the expression of other iron homeostasis proteins such as iron-response element protein 1/2 (IRP1/2), ferroportin (FPN), and divalent metal transporter (DMT1) was unaffected by iron loading in none of the groups (Fig. 3b–e). In contrast, the protein level of ferritin, a cytosolic iron storage and detoxification protein, increased upon iron loading in both FRDA- and WT-iPSC cardiomyocytes. Similar to TSFR gene expression, the rise in ferritin upon iron loading was smaller in FRDA-iPSC cardiomyocytes than in WT cells (23.40±8.52 vs. 56.47±15.72 %, significant difference was found between two iron-loaded groups, $p<0.05$), indicating defects in buffering of toxic intracellular iron (Fig. 3f).

Mitochondrial ATP synthesis

As frataxin deficiency results in impaired iron–sulfur cluster biogenesis thereby possibly affecting ATP production, we studied the mitochondrial ATP synthesis in cardiomyocytes derived from FRDA- and WT-iPSCs. Cells were SLO-permeabilized to remove cytosolic content and treated with respiratory substrates such as succinate and ADP. The amount of ATP synthesized was continuously measured as real-time luminescence signal by a luminometer microplate reader. Under normal culture condition, the basal rates of ATP production of FRDA-iPSC-derived cardiomyocytes did not differ from the WT counterpart (22,965±3,203 normalized luciferase light unit/min vs. 17,918±1,693 normalized luciferase light unit/min, $n=6$), which increased linearly with time (Fig. 4). With the addition of iron (II) sulfate, there was no difference in rate of ATP production in WT iPSC cardiomyocytes. In stark contrast, iron treatment resulted in a 26 % reduction in ATP production in FRDA-iPSC cardiomyocytes ($n=6$, *$p<0.05$) (Fig. 4b).

Calcium handling in FRDA-iPSC cardiomyocytes

To assess the functional consequences of iron homeostasis abnormalities in FRDA cardiomyocytes, we measured the calcium transients which are key elements of the excitation–contraction coupling. Resembling wild-type iPSC cardiomyocytes, spontaneous rhythmic calcium transients were observed in FRDA-iPSC cardiomyocytes (Fig. 5a). As shown in Fig. 5b, WT- and FRDA-iPSC cardiomyocytes exhibited comparable calcium transient amplitude and decay time. Interestingly, after iron treatment, marked impairment of calcium homeostasis was observed in FRDA-iPSC cardiomyocytes but not in wild-type iPSC counterpart. The rise time of spontaneous rhythmic calcium transients of FRDA-iPSC cardiomyocytes modestly increased with a significant difference at $p<0.05$ with iron treatment, and the decay time was elevated for approximately 40 % after treatment (639±48.27 vs. 890±80 ms, **$p<0.005$, $n=20$). Such changes were not observed in the wild-type group (Fig. 5b). Moreover, the caffeine-induced release of SR Ca^{2+} is also obviously diminished for 2-folds in iron-treated FRDA-iPSC cardiomyocytes ($n=15$; *$p<0.05$) (Fig. 5c, d) with diastolic intracellular Ca^{2+} surge for more than 3-folds comparing with wild-type cells treated with iron ($n=30$; ***$p<0.001$)

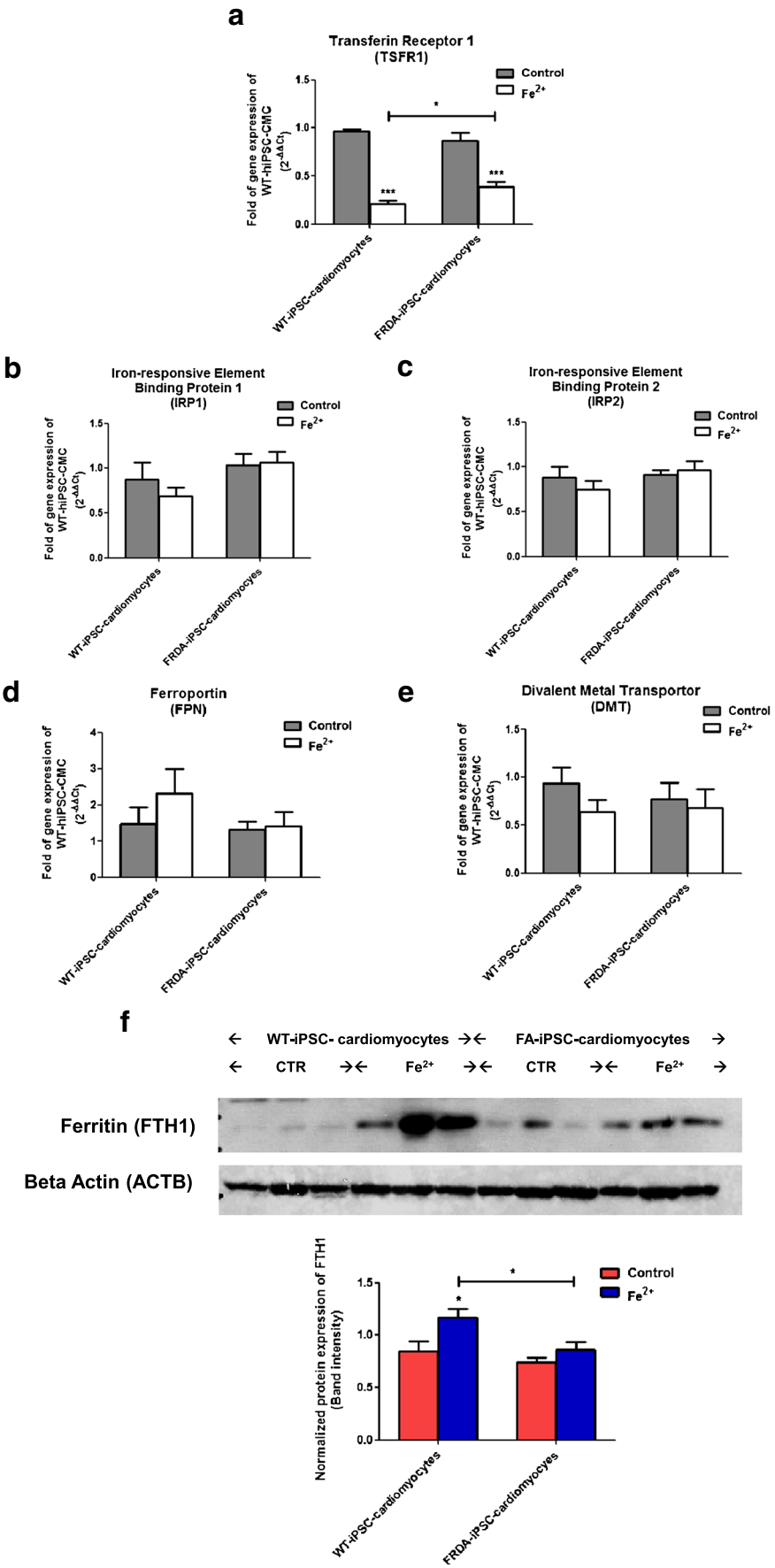

Fig. 3 **a** Decline in transferrin receptor (TSFR) gene expression of FRDA-iPSC-CMC is more susceptible to iron (II) treatment. qPCR determination of gene level was calculated by the ΔΔCt method with the treatment group compared with baseline of each cell line. Transferrin receptor (TSFR), the transferrin-bound Fe importer, was significantly reduced upon iron (II) stress in both WT- and FRDA-iPSC-CMCs, while FRDA cells were less vulnerable to the treatment ($n=6$, $^{***}p<0.001$); **b**–**e** gene expression levels of iron-response element binding protein 1/2 (IRP1/2), the iron exporters, ferroportin (FPN), and divalent metal ion transportor-1 (DMT1) remained unchanged under iron-loading stress. **f** Attenuated upregulation of ferritin (FTH1) level in FRDA-iPSC cardiomyocytes in response to iron (II) stress. Protein expressions of FTH1 are normalized to beta-actin expression. Significant difference was shown at $^{*}p<0.05$, $n=6$

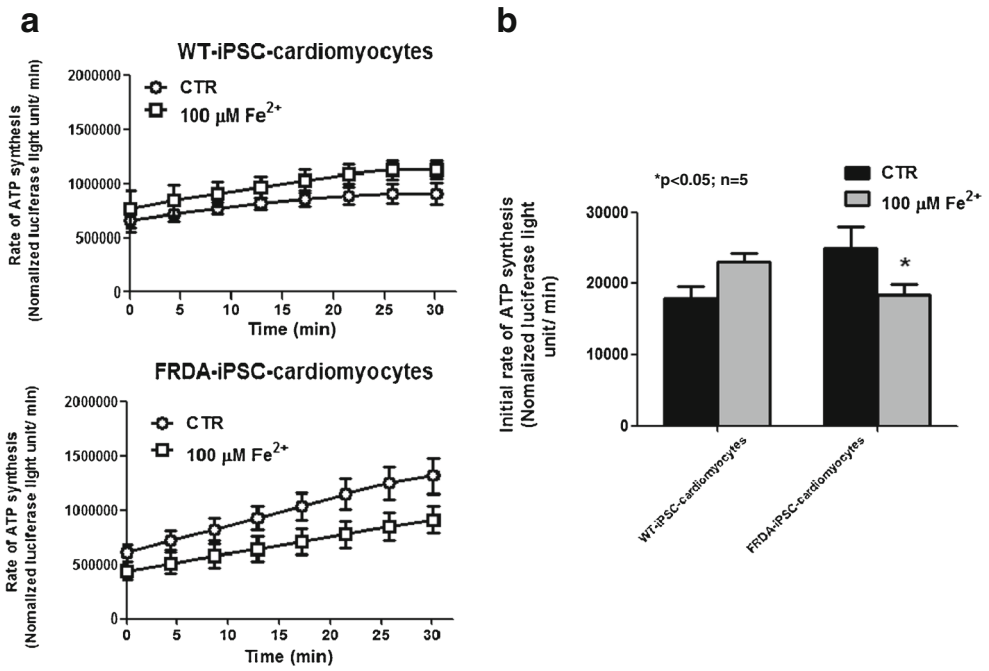

Fig. 4 **a**, **b** Iron overload suppressed mitochondrial ATP synthesis in FRDA-iPSC cardiomyocytes. The kinetics of ATP synthesis by mitochondrial was analyzed in terms of initial upstroke velocity of ATP-driven luciferase activity (significant difference was tested by unpaired *t* test; $n=5$; $*p<0.05$)

(Fig. 5e). Despite the impairment of calcium homeostasis in iron-treated FRDA-iPSC cardiomyocytes, the expression of sarcoplasmic reticulum calcium ATPase 2a (SERCA-2a) was similar in both WT and FA hiPSC cardiomyocytes under basal and iron (II) condition (Fig. 5f). However, other gene expression of major calcium handling proteins ryanodine receptor 2 (RyR2) was increased in the FA group at basal condition in comparison with WT which was reflected with modest increase calcium transient rising kinetics of FRDA-hiPSC cardiomyocytes. Finally, both groups of the WT-hiPSC cardiomyocytes were responsive to beta-adrenergic stimulation since the addition of isoproterenol (10 μM) caused a positive inotropic effect (Fig. 5g, h). FRDA-cardiac cells in both baseline and iron overload conditions were barely responsive to adrenergic stimulation implying that a defect in SR function arose even in baseline condition. Quantitatively, the frequency changes of WT-hiPSC cardiomyocytes were from basal condition at 259.3±52.21 % to iron (II)-treated condition with 175.71±7.94 % (percent changes of baseline), while FRDA-hiPSC cardiomyocytes changed from 58±7.95 to 45.13±7.29 %. Significant difference was analyzed between basal- and iron-loaded condition between WT and FRDA cells ($n=8$, $***p<0.0001$).

Discussion

Nearly all FRDA patients eventually develop cardiomyopathy, and the resultant heart failure is considered to be the primary cause of death in approximately 60 % of FRDA patients [23]. While GAA triplet repeat expansions in first intron of *FXN* gene resulting in heterochromatin-mediated silencing have been found in the majority of FRDA patients [36], the pathogenic link between frataxin deficiency and the development of cardiomyopathy and subsequent heart failure remains elusive.

In order to provide insights to the underlying cardiac pathogenesis in FRDA, in the present study, we have established FRDA-specific iPSC lines and differentiated them into cardiac derivatives for ex vivo functional testing. During the generation of iPSC from a FRDA patient, there was an expansion of first intronic GAA triplet repeat in *FXN* gene. A similar expansion has also been observed in a recent report by Ku and co-workers [14]. It has also been suggested that the mismatch repair enzyme, MSH2, may play a role in the GAA repeat instability in pluripotent cells [14]. Despite the presence of disorganized mitochondrial network and reduced level of mitochondrial DNA in FRDA-iPSC cardiomyocytes, these mutated cardiomyocytes were similar to the WT group in terms of cell size, ATP production rate, and calcium transient properties. However, when these cells were cultured in the presence of excessive iron supplement, they exhibited hypertrophic changes, reduced ATP production, and impaired calcium handling properties. Additionally, markedly enhanced iron uptake through the attenuated negative feedback of the transferrin-mediated iron uptake was also observed in FRDA-iPSC cardiomyocytes.

Currently, insights into the pathogenesis of FRDA-related cardiomyopathy are largely based on the presumed functional roles of frataxin and observations from clinical studies and

experimental animal models. Given the presumptive role of frataxin in the biogenesis of iron–sulfur cluster, an essential component of enzymes in respiratory electronic transport chain, it is plausible to suggest that impaired energy generation serves as a major pathogenic mechanism underlying FRDA-related cardiomyopathy. Indeed, impaired activity of enzymes in electron transport chain such as complexes I, II, and III has been demonstrated in myocardial tissues obtained from FRDA patients [27]. Consistently, phosphorus magnetic resonance spectroscopy studies have shown a reduced ATP production in the hearts of FRDA patients [2]. More importantly, the extent of myocardial energy deficiency in FRDA patients has then been shown to correlate strongly with the degree of left ventricular hypertrophy, thus supporting the significance of impaired energy production in the pathogenesis of FRDA-related cardiomyopathy [4]. However, there are also important arguments to suggest additional and/or alternative mechanisms for the development of hypertrophic cardiomyopathy in FRDA. For example, while frataxin deficiency and the presumed reduction of ATP production occur early on in life, patients with FRDA are born with normally functioning heart, and left ventricular hypertrophy and systolic dysfunction are not commonly observed in young FRDA patients until adulthood [13]. In fact, similar observations have also been made in the muscle creatine kinase (MCK) conditional frataxin knock-out mouse model that reproduces the classical traits of FRDA-related cardiomyopathy [24, 33]. Specifically, animals with MCK conditional deletion of frataxin exhibited no visible cardiac phenotype at 4 weeks, but developed typical cardiomyopathic changes at 9 weeks of age. In concordance with these observations, a very recent study modeling FRDA using iPSC technology [10] and our results showed that under conventional culture condition, cardiomyocytes derived from FRDA patients, despite the presence of mitochondrial abnormalities, exhibited other structural, biochemical, or functional signs of cardiomyopathy. This suggests that frataxin deficiency per se does not suffice to impair energy production in FRDA cardiomyocytes, or to induce cardiomyopathic changes in FRDA.

In addition to the energy deficiency, myocardial iron accumulation has also been suggested to play a role in the development of cardiomyopathy in FRDA. For instance, myocardial iron accumulation has been observed in the heart of FRDA patients for more than 30 years [16], and the biochemical features of FRDA-related cardiomyopathy such as reduced activities of complexes I, II, and III and aconitase mentioned previously were often observed in the presence of myocardial iron accumulation [2]. Albeit this, iron accumulation has often been considered not instrumental or as a late event in the pathogenesis of FRDA [1]. This is at least partly related to the failure to document iron accumulation in skin fibroblasts or lymphoblasts from patients with FRDA [29]. Even in the hearts of patients with FRDA, iron accumulation has not been consistently demonstrated [21]. However, a recent work by Ramirez and co-workers studying the whole heart specimens from FRDA patients has reconciled this inconsistency that instead of the diffuse nature as observed in hemochromatosis, iron accumulation in the FRDA heart is focal in nature, and preferentially affects the subendocardial working myocardium [25]. This may explain the lack of myocardial iron accumulation particularly from studies using blind random endomyocardial biopsied specimens or chemical assays of iron in bulk extracts of tissue. Even so, at the whole organism level, it is often difficult, if not impossible, to dissect the contributory effects of individual factors on the pathogenesis. Using the human iPSC cardiomyocyte platform, it is not only possible to study the functionality of live cardiomyocytes, which has not been technically feasible in most circumstances; it allows manipulations of individual mechanisms and pathways in order to investigate their relative importance. As demonstrated in our study, in the absence of an iron supplement, FRDA cardiomyocytes exhibited no evidence of impaired energy production, calcium handling, or any hypertrophic changes as compared with wild-type cardiomyocytes, despite documented mitochondrial abnormalities. However, when supplemented with iron, FRDA cardiomyocytes exhibited hypertrophic changes with impaired ATP production and calcium handling. These findings highlight the central role of iron accumulation in the pathogenesis of FRDA cardiomyopathy and specifically suggested that iron loading led to functionally worsened calcium handling in FRDA-iPSC-CM regardless of transcriptional alternation in calcium handling protein, particularly affected in the phase of decay in calcium transient that involved SERCA, which was highly dependent on ATP supply due to pumping

Fig. 5 Functional properties in the iron-loaded FRDA-iPSC cardiomyocytes. **a** Representative tracing of calcium transients in WT- and FRDA-iPSC cardiomyocytes with iron (II) treatment; **b** the maximum calcium released (amplitude), rise time from 50 to 100 % of peak amplitude (milliseconds), and decay time from 100 to 50 % of peak amplitude (milliseconds) (*$p<0.05$, **$p<0.005$, and ***$p<0.0001$ compared to baseline of the same cell group) from 15 to 20 samples were presented. The iron overloaded FRDA-iPSC-CMC presented a suppressed rate of calcium release and uptake; **c** representative tracing of caffeine-induced calcium release in WT- and FRDA-iPSC cardiomyocytes with iron (II) treatment; *arrows* indicated the time of caffeine (10 mM) addition. **d** The maximum calcium released (amplitude). The maximum calcium released (amplitude), rise time from 50 to 100 % of peak amplitude (milliseconds) and decay time from 100 to 50 % of peak amplitude (milliseconds) (*$p<0.05$, **$p<.005$, and ***$p<0.0001$ compared to baseline of the same cell group) from 10 samples were presented; **e** diastolic calcium level of WT- and FRDA-iPSC cardiomyocytes with iron (II) treatment The concentration was determined with K_d=422 nM (n=30; *$p<0.05$ and ***$p<0.0001$ compared to baseline indicated). **f** Transcriptional levels of the calcium handling proteins in FRDA-iPSC-CMC with iron (II) treatment (n=); **g**, **h** attenuated responsiveness to beta-adrenergic stimulation in FRDA-iPSC cardiomyocytes (*arrows*: time for addition of 10 μM isoproterenol)

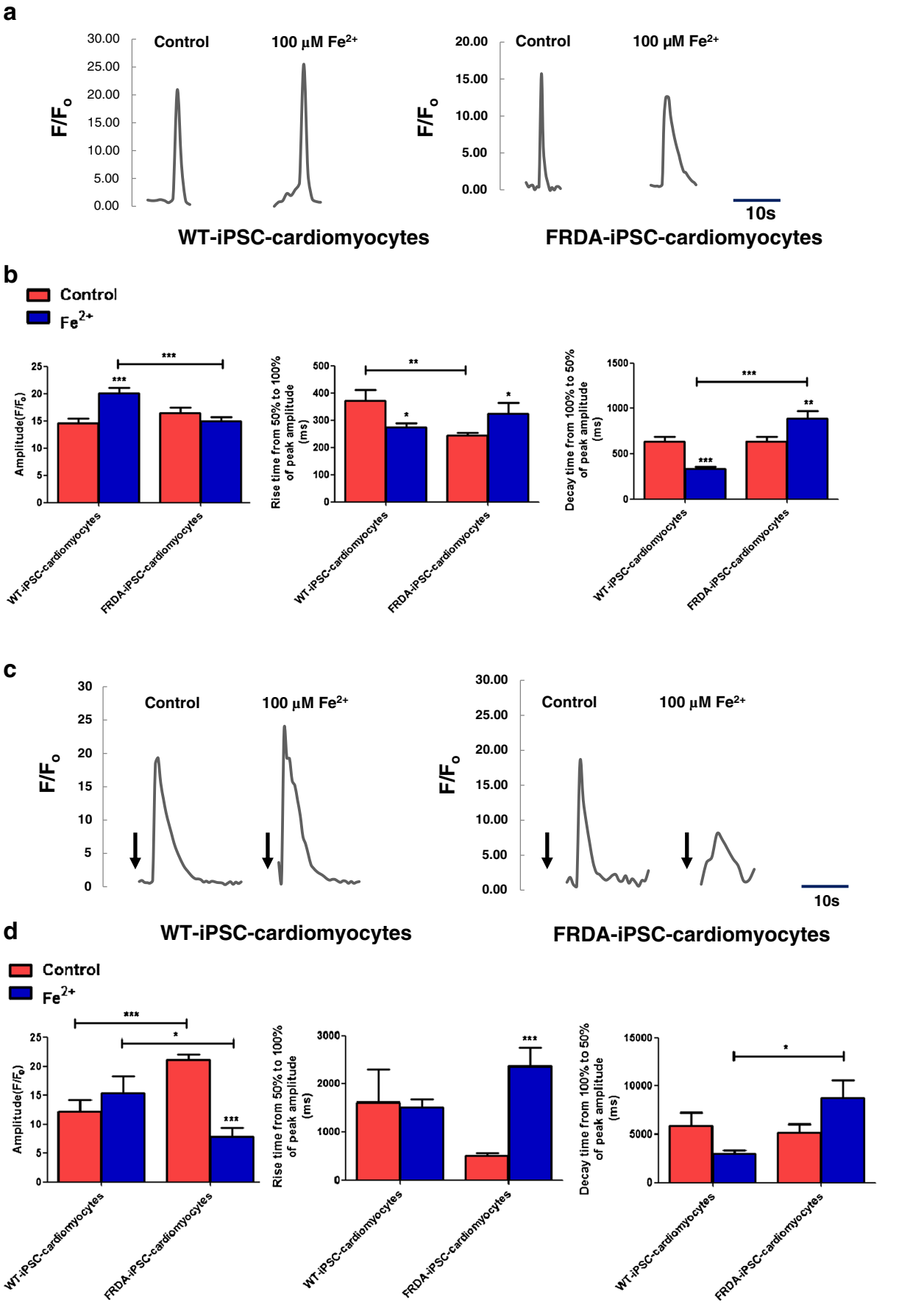
a
Control
100 µM Fe2+
F/Fo
30.00
25.00
20.00
15.00
10.00
5.00
0.00
20.00
15.00
10.00
5.00
0.00
10s
WT-iPSC-cardiomyocytes
FRDA-iPSC-cardiomyocytes
b
Control
Fe2+
Amplitude(F/Fo)
Rise time from 50% to 100% of peak amplitude (ms)
Decay time from 100% to 50% of peak amplitude (ms)
WT-iPSC-cardiomyocytes
FRDA-iPSC-cardiomyocytes
c
Control
100 µM Fe2+
F/Fo
10s
WT-iPSC-cardiomyocytes
FRDA-iPSC-cardiomyocytes
d
Control
Fe2+
Amplitude(F/Fo)
Rise time from 50% to 100% of peak amplitude (ms)
Decay time from 100% to 50% of peak amplitude (ms)
WT-iPSC-cardiomyocytes
FRDA-iPSC-cardiomyocytes

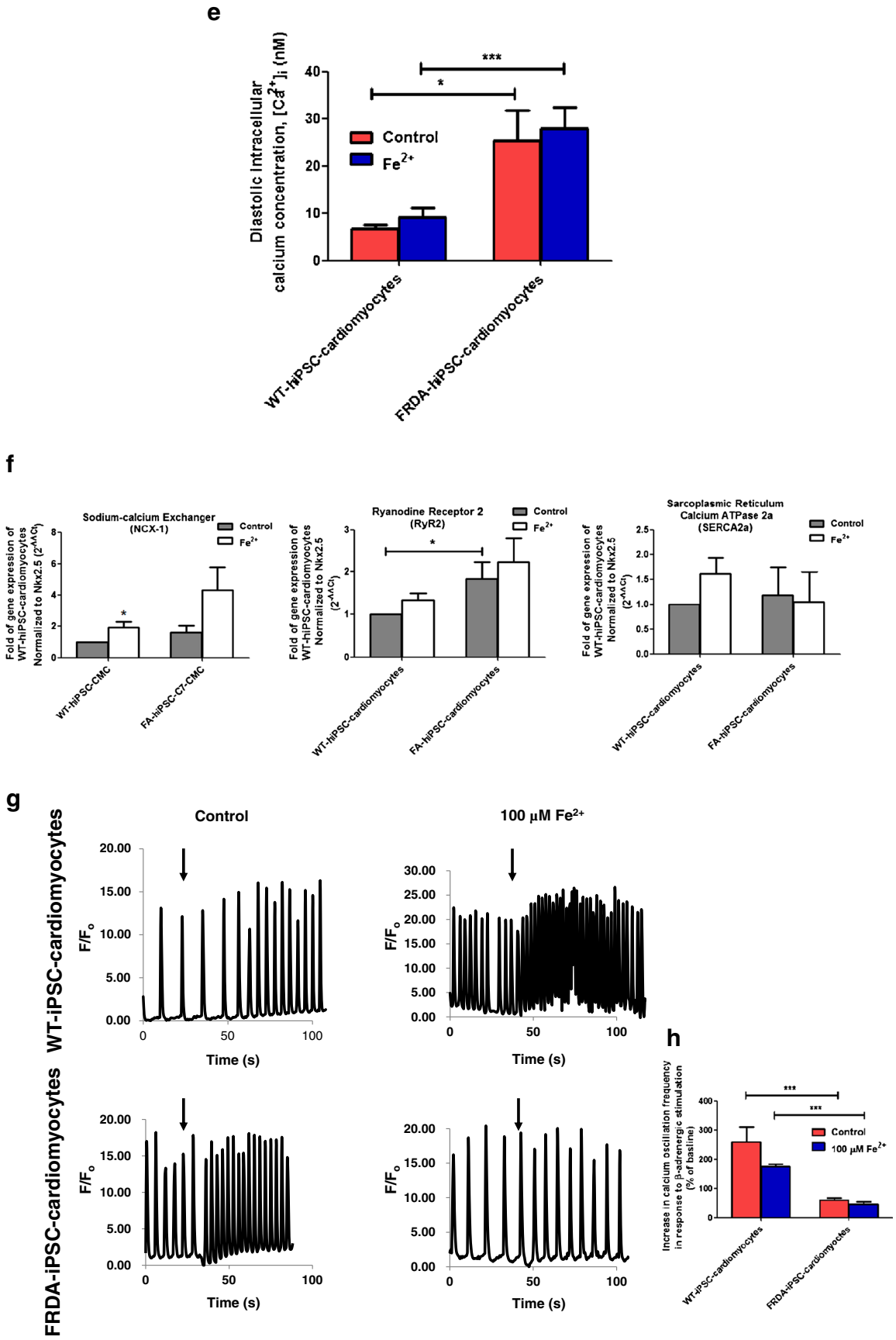

Fig. 5 (continued)

of Ca^{2+} against concentration gradient (from the cytosol back into SR) and subsequently also diminished SR Ca^{2+} load due to metabolic insufficiency. In fact, a therapeutic strategy targeting myocardial iron accumulation has been explored [33]. It has been shown in the MCK conditional frataxin knock-out mouse model that the use of iron chelating therapy such as desferrioxamine effectively prevented myocardial iron accumulation loading and alleviated cardiac hypertrophy without restoring the reduced level of electron transport chain enzyme [33].

Under normal circumstances, intracellular iron content is under tight homeostatic control. For instance, when iron level is low, cytosolic iron response protein (IRP) 1 and 2 bind to 5′ and 3′ ends of the iron-responsive elements in mRNAs encoding iron regulating proteins such as transferrin receptor (TSFR), divalent metal transporter (DMT1), and ferroportin (FPN) and stabilize them, thereby increasing iron uptake. When intracellular iron level is high, IRP1 incorporates with iron sulfur clusters to interfere the binding of IRP to iron-responsive elements, thus preventing further increase in intracellular iron [11, 32]. In our study, when cultured with iron supplement, the cellular iron content in WT cardiomyocytes remained unchanged with appropriate suppression of the expression of TSFR and increase in ferritin level. In marked contrast, the cellular iron content in FRDA cardiomyocytes increased by approximately 7,500-folds with much attenuated reduction in TSFR and increase in ferritin, reflecting a blunted negative feedback to increase in iron content.

This study has several limitations. First, due to the lack of skin biopsy sample from patients with FRDA, we were only able to obtain iPSC and its cardiac derivatives from a single FRDA patient. In fact, we did not observe any significant batch-to-batch variation in iPSC and cardiomyocytes obtained from the same individual. Second, cardiomyocytes derived from human iPSC resemble at most neonatal cardiomyocytes with immature phenotypes. Moreover, under culture conditions, it would be difficult, if not impossible, to mimic all in vivo physiological environments such as hemodynamic loading. Nonetheless, human iPSC-derived cardiomyocytes remain the closet human platform that allows in vitro functional testing at this point in time.

Taken collectively, frataxin deficiency and the associated iron–sulfur cluster deficiency per se are not sufficient to alter the basal rate of energy production, as well as calcium handling, the prime function of cardiomyocytes. However, the compensatory mechanisms to enhance iron uptake leading to myocardial iron accumulation adversely affect normal cardiomyocyte function. This may explain the degenerative nature of the disease that the occurrence of heart failure in FRDA patients is usually late approx. two to three decades of life, which may be the time needed for the cardiomyocytes to accumulate adequate iron under normal iron concentration. Third, concerning the iron-induced alteration of calcium handling properties in FRDA-iPSC cardiomyocytes, while the expressions of a panel of calcium handing protein gene changed upon a 48-h iron treatment, a definite conclusion can only be drawn with quantitative documentation of the corresponding changes of the protein levels. Given the small number of cardiomyocyte-obtained FRDA-iPSC, it would not be possible at this moment.

Conclusion

We have successfully established FRDA-specific human iPSC platform as a disease model for FRDA-related cardiomyopathy. The current study provides novel findings in the pathogenic mechanism of FRDA: (1) under normal culture condition, WT- and FRDA-iPSC-CMCs showed no variation in terms of cardiac function and mitochondrial activity; (2) mitochondrial ATP synthesis activity is highly vulnerable to iron loading stress in FRDA-iPSC-CMCs; (3) excitation contraction coupling (EC) function of FRDA-iPSC-CMCs was impaired under stress due to a lack for ATP source for Ca^{2+} reuptake function as well as mechanical movement of myofilaments; (4) the response of transferrin receptor (TSFR) suppression and ferritin (FTH) elevation was reduced in FRDA-iPSC-CMs upon iron loading stress.

Acknowledgments This work was supported by grants from the Hong Kong Research Grant Council (HKU 776912 M to Drs. Siu and Lau) and Israel Science Foundation, The Ministry of Health—Chief Scientist, the Rappaport Family Institute for Research in the Medical Sciences, and The Sohnis and Forman Families Stem Cells Center (to Ofer Binah).

Conflict of Interest The authors have nothing to disclose.

References

1. Bayot A, Santos R, Camadro JM, Rustin P (2011) Friedreich's ataxia: the vicious circle hypothesis revisited. BMC Med 9:112. doi:10.1186/1741-7015-9-112
2. Bradley JL, Blake JC, Chamberlain S, Thomas PK, Cooper JM, Schapira AH (2000) Clinical, biochemical and molecular genetic correlations in Friedreich's ataxia. Hum Mol Genet 9:275–82
3. Bradley JL, Blake JC, Chamberlain S, Thomas PK, Cooper JM, Schapira AH (2000) Clinical, biochemical and molecular genetic correlations in Friedreich's ataxia. Human molecular genetics 9: 275–82
4. Bunse M, Bit-Avragim N, Riefflin A, Perrot A, Schmidt O, Kreuz FR, Dietz R, Jung WI, Osterziel KJ (2003) Cardiac energetics correlates to myocardial hypertrophy in Friedreich's ataxia. Ann Neurol 53:121–3. doi:10.1002/ana.10419
5. Campuzano V, Montermini L, Molto MD, Pianese L, Cossee M, Cavalcanti F, Monros E, Rodius F, Duclos F, Monticelli A, Zara F, Canizares J, Koutnikova H, Bidichandani SI, Gellera C, Brice A, Trouillas P, De Michele G, Filla A, De Frutos R, Palau F, Patel PI, Di Donato S, Mandel JL, Cocozza S, Koenig M, Pandolfo M (1996)

Friedreich's ataxia: autosomal recessive disease caused by an intronic GAA triplet repeat expansion. Science 271:1423–7
6. Chantrel-Groussard K, Geromel V, Puccio H, Koenig M, Munnich A, Rotig A, Rustin P (2001) Disabled early recruitment of antioxidant defenses in Friedreich's ataxia. Hum Mol Genet 10:2061–7
7. Fujikawa M, Yoshida M (2010) A sensitive, simple assay of mitochondrial ATP synthesis of cultured mammalian cells suitable for high-throughput analysis. Biochem Biophys Res Commun 401:538–43. doi:10.1016/j.bbrc.2010.09.089
8. Geoffroy G, Barbeau A, Breton G, Lemieux B, Aube M, Leger C, Bouchard JP (1976) Clinical description and roentgenologic evaluation of patients with Friedreich's ataxia. Can J Neurol Sci 3:279–86
9. Herman D, Jenssen K, Burnett R, Soragni E, Perlman SL, Gottesfeld JM (2006) Histone deacetylase inhibitors reverse gene silencing in Friedreich's ataxia. Nat Chem Biol 2:551–8. doi:10.1038/nchembio815
10. Hick A, Wattenhofer-Donze M, Chintawar S, Tropel P, Simard JP, Vaucamps N, Gall D, Lambot L, Andre C, Reutenauer L, Rai M, Teletin M, Messaddeq N, Schiffmann SN, Viville S, Pearson CE, Pandolfo M, Puccio HM (2013) Induced pluripotent stem cell derived neurons and cardiomyocytes as a model for mitochondrial defects in Friedreich's ataxia. Dis Model Mech 6(3):608–612. doi:10.1242/dmm.010900
11. Horowitz MP, Greenamyre JT (2010) Mitochondrial iron metabolism and its role in neurodegeneration. J Alzheimers Dis 20(Suppl 2): S551–68
12. Huang ML, Becker EM, Whitnall M, Suryo Rahmanto Y, Ponka P, Richardson DR (2009) Elucidation of the mechanism of mitochondrial iron loading in Friedreich's ataxia by analysis of a mouse mutant. Proc Natl Acad Sci U S A 106:16381–6. doi:10.1073/pnas.0906784106
13. Kipps A, Alexander M, Colan SD, Gauvreau K, Smoot L, Crawford L, Darras BT, Blume ED (2009) The longitudinal course of cardiomyopathy in Friedreich's ataxia during childhood. Pediatr Cardiol 30: 306–10. doi:10.1007/s00246-008-9305-1
14. Ku S, Soragni E, Campau E, Thomas EA, Altun G, Laurent LC, Loring JF, Napierala M, Gottesfeld JM (2010) Friedreich's ataxia induced pluripotent stem cells model intergenerational GAATTC triplet repeat instability. Cell Stem Cell 7:631–7. doi:10.1016/j.stem.2010.09.014
15. Lai WH, Ho JC, Lee YK, Ng KM, Au KW, Chan YC, Lau CP, Tse HF, Siu CW (2010) ROCK inhibition facilitates the generation of human-induced pluripotent stem cells in a defined, feeder-, and serum-free system. Cell Reprogram 12:641–53. doi:10.1089/cell.2010.0051
16. Lamarche JB, Cote M, Lemieux B (1980) The cardiomyopathy of Friedreich's ataxia morphological observations in 3 cases. Can J Neurol Sci 7:389–96
17. Lee YK, Ng KM, Lai WH, Chan YC, Lau YM, Lian Q, Tse HF, Siu CW (2011) Calcium homeostasis in human induced pluripotent stem cell-derived cardiomyocytes. Stem Cell Rev 7:976–86. doi:10.1007/s12015-011-9273-3
18. Lian Q, Zhang Y, Zhang J, Zhang HK, Wu X, Lam FF, Kang S, Xia JC, Lai WH, Au KW, Chow YY, Siu CW, Lee CN, Tse HF (2010) Functional mesenchymal stem cells derived from human induced pluripotent stem cells attenuate limb ischemia in mice. Circulation 121:1113–23. doi:10.1161/CIRCULATIONAHA.109.898312
19. Liu J, Verma PJ, Evans-Galea MV, Delatycki MB, Michalska A, Leung J, Crombie D, Sarsero JP, Williamson R, Dottori M, Pebay A (2011) Generation of induced pluripotent stem cell lines from Friedreich ataxia patients. Stem Cell Rev 7:703–13. doi:10.1007/s12015-010-9210-x
20. Martelli A, Wattenhofer-Donze M, Schmucker S, Bouvet S, Reutenauer L, Puccio H (2007) Frataxin is essential for extramitochondrial Fe-S cluster proteins in mammalian tissues. Human molecular genetics 16:2651–8. doi:10.1093/hmg/ddm163
21. Michael S, Petrocine SV, Qian J, Lamarche JB, Knutson MD, Garrick MD, Koeppen AH (2006) Iron and iron-responsive proteins in the cardiomyopathy of Friedreich's ataxia. Cerebellum 5:257–67. doi:10.1080/14734220600913246
22. Payne RM (2011) The heart in Friedreich's ataxia: basic findings and clinical implications. Prog Pediatr Cardiol 31:103–109. doi:10.1016/j.ppedcard.2011.02.007
23. Payne RM, Wagner GR (2012) Cardiomyopathy in Friedreich ataxia: clinical findings and research. J Child Neurol 27:1179–86. doi:10.1177/0883073812448535
24. Puccio H, Simon D, Cossee M, Criqui-Filipe P, Tiziano F, Melki J, Hindelang C, Matyas R, Rustin P, Koenig M (2001) Mouse models for Friedreich ataxia exhibit cardiomyopathy, sensory nerve defect and Fe–S enzyme deficiency followed by intramitochondrial iron deposits. Nature genetics 27:181–6. doi:10.1038/84818
25. Ramirez RL, Qian J, Santambrogio P, Levi S, Koeppen AH (2012) Relation of cytosolic iron excess to cardiomyopathy of Friedreich's ataxia. Am J Cardiol 110:1820–7. doi:10.1016/j.amjcard.2012.08.018
26. Rindler PM, Clark RM, Pollard LM, De Biase I, Bidichandani SI (2006) Replication in mammalian cells recapitulates the locus-specific differences in somatic instability of genomic GAA triplet-repeats. Nucleic Acids Res 34:6352–61. doi:10.1093/nar/gkl846
27. Rotig A, de Lonlay P, Chretien D, Foury F, Koenig M, Sidi D, Munnich A, Rustin P (1997) Aconitase and mitochondrial iron–sulphur protein deficiency in Friedreich ataxia. Nature genetics 17: 215–7. doi:10.1038/ng1097-215
28. Schulz JB, Boesch S, Burk K, Durr A, Giunti P, Mariotti C, Pousset F, Schols L, Vankan P, Pandolfo M (2009) Diagnosis and treatment of Friedreich ataxia: a European perspective. Nat Rev Neurol 5:222–34
29. Sturm B, Bistrich U, Schranzhofer M, Sarsero JP, Rauen U, Scheiber-Mojdehkar B, de Groot H, Ioannou P, Petrat F (2005) Friedreich's ataxia, no changes in mitochondrial labile iron in human lymphoblasts and fibroblasts: a decrease in antioxidative capacity? J Biol Chem 280:6701–8. doi:10.1074/jbc.M408717200
30. Sun N, Yazawa M, Liu J, Han L, Sanchez-Freire V, Abilez OJ, Navarrete EG, Hu S, Wang L, Lee A, Pavlovic A, Lin S, Chen R, Hajjar RJ, Snyder MP, Dolmetsch RE, Butte MJ, Ashley EA, Longaker MT, Robbins RC, Wu JC (2012) Patient-specific induced pluripotent stem cells as a model for familial dilated cardiomyopathy. Sci Transl Med 4:130ra47 DOI 4/130/130ra47 [pii] 10.1126/scitranslmed.3003552
31. Takahashi K, Tanabe K, Ohnuki M, Narita M, Ichisaka T, Tomoda K, Yamanaka S (2007) Induction of pluripotent stem cells from adult human fibroblasts by defined factors. Cell 131:861–72. doi:10.1016/j.cell.2007.11.019
32. Wallander ML, Leibold EA, Eisenstein RS (2006) Molecular control of vertebrate iron homeostasis by iron regulatory proteins. Biochim Biophys Acta 1763:668–89. doi:10.1016/j.bbamcr.2006.05.004
33. Whitnall M, Suryo Rahmanto Y, Sutak R, Xu X, Becker EM, Mikhael MR, Ponka P, Richardson DR (2008) The MCK mouse heart model of Friedreich's ataxia: alterations in iron-regulated proteins and cardiac hypertrophy are limited by iron chelation. Proc Natl Acad Sci U S A 105:9757–62. doi:10.1073/pnas.0804261105
34. Yu J, Vodyanik MA, Smuga-Otto K, Antosiewicz-Bourget J, Frane JL, Tian S, Nie J, Jonsdottir GA, Ruotti V, Stewart R, Slukvin II, Thomson JA (2007) Induced pluripotent stem cell lines derived from human somatic cells. Science 318:1917–20. doi:10.1126/science.1151526
35. Zhang J, Lian Q, Zhu G, Zhou F, Sui L, Tan C, Mutalif RA, Navasankari R, Zhang Y, Tse HF, Stewart CL, Colman A (2011) A human iPSC model of Hutchinson Gilford Progeria reveals vascular smooth muscle and mesenchymal stem cell defects. Cell Stem Cell 8: 31–45. doi:10.1016/j.stem.2010.12.002
36. Zuhlke CH, Dalski A, Habeck M, Straube K, Hedrich K, Hoeltzenbein M, Konstanzer A, Hellenbroich Y, Schwinger E (2004) Extension of the mutation spectrum in Friedreich's ataxia: detection of an exon deletion and novel missense mutations. Eur J Hum Genet 12:979–82. doi:10.1038/sj.ejhg.52012575201257